J Mater Sci (2006) 41:5828–5835
DOI 10.1007/s10853-006-0299-x

Effect of electrodes and zeolite cover layer on hydrocarbon sensing with *p*-type perovskite $SrTi_{0.8}Fe_{0.2}O_{3-\delta}$ thick and thin films

Kathy Sahner · Daniela Schönauer · Ralf Moos · Mahesh Matam · Michael L. Post

Received: 28 July 2005 / Accepted: 7 October 2005 / Published online: 28 June 2006
© Springer Science+Business Media, LLC 2006

Abstract Screen-printed thick film as well as pulsed laser deposited thin film sensors of the perovskite $SrTi_{0.8}Fe_{0.2}O_{3-\delta}$ (STF20) with gold electrodes present poor hydrocarbon selectivity when exposed to different gases (hydrocarbons, hydrogen, NO, and CO). By employing Pt-electrodes, response to H_2 and CO is eliminated. In the case of thick film devices, only NO cross interference persists. The selectivity of the thick films is further increased by applying a Pt doped zeolite (ZSM-5) as a cover layer. By adjusting the thickness of the ZSM-5 cover layer, the film selectively senses mainly saturated hydrocarbons such as propane, suppressing the response towards all the other gases. This effect is attributed to the catalytic effect of the high Pt-content of the ZSM-5 zeolite. Application of a ZSM-5 cover layer to thin films enhances the sensor output response to propane, thus reducing selectivity for unsaturated hydrocarbons. A sensor configuration having Pt electrodes on top of an STF20 thick film with an additional 50 μm cover layer of ZSM-5 was found to be the most suitable to selectively sense saturated hydrocarbons. Thin film STF20 sensors equipped with Pt-IDC electrodes and without the zeolite cover layer, were found to perform best for unsaturated hydrocarbons at 400°C.

K. Sahner (✉) · D. Schönauer · R. Moos
Functional Materials, University of Bayreuth, 95447 Bayreuth, Germany
e-mail: Funktionsmaterialien@uni-bayreuth.de

M. Matam · M. L. Post
Institute for Chemical Process and Environmental Technology, National Research Council of Canada, 1200 Montreal Road, K1A 0R6 Ottawa, Canada

Introduction

The need to reduce emissions and pollutants that are hazardous or cause global warming is continuously increasing, and this necessitates determining strategies for identifying and eliminating them effectively. Various governments accepting the 'Kyoto protocol' have set new limitations on such emissions, with the resulting demand to chemically sense these gases increasing at a consistent pace. Severe environmental conditions and miniaturization have put new requirements on sensors. Thus, they not only need to selectively sense one particular gas [1], but also must be robust and withstand changing ambient environments. To sense hazardous gases, conductometric metal oxide sensors, such as those based on SnO_2 [2, 3] and ZnO [4, 5] have been investigated for many years.

One feature that is common to most of the metal oxide gas sensors is that they are *n*-type semiconductors, where the resistance decreases as a function of the applied reducing gas partial pressure. However effective they are, their performance is still limited by various factors such as humidity, poor selectivity, high error margins, non-retention of the base value upon cycling etc. [6, 7]. Thus, it becomes necessary to seek alternate materials that either have better performance than, or are complementary to, the *n*-type metal-oxide sensors.

As an alternative, *p*-type semiconductors have been shown to be effective gas sensors, which are rugged and robust and do not suffer from some of the limitations of *n*-type semiconductors [8]. Some of these sensors are already commercially available, for example, ammonia sensors of $Cr_{2-x}Ti_xO_3$ [9, 10], and rare-earth metal-oxide based $LnFeO_3$ perovskite sensors for NO_x detection, where Ln = La, Sm, Gd, and Dy [11]. Even so, the investigation of *p*-type semiconducting oxides for gas sensing applications is limited, despite the advantages they possess when compared to *n*-type sensors. In an effort to find new materials based on *p*-type semiconducting perovskites for gas sensing applications, sensors based on perovskite $SrTi_{1-x}Fe_xO_{3-\delta}$ (STFx, where *x* denotes the Fe content), which present higher catalytic activity than the *n*-type sensors, have recently been investigated [12]. It has been demonstrated earlier that this family of materials are promising candidates for hydrocarbon sensing in the temperature range from 350 to 450°C. In this context, an initial model based on a diffusion-reaction process was proposed in order to describe the underlying sensing mechanism [13].

The present contribution focuses on a particular member of this *p*-type conducting semiconductor family, namely STF20. Sensor films have been fabricated using thin and thick film processing techniques, and their corresponding sensor functionality has been compared and contrasted. A number of sensor fabrication features have been studied with respect to consequences on sensor functionality. An example is using different electrode metals, Au and Pt, deposited as interdigitated capacitive (IDC) structures. The advantages of using either of them is discussed with reference to the catalytic activity that they may induce. Also studied in the case of the STF20 thick film sensors, are various types of electrode configurations, with electrodes being deposited either on top or beneath the film. In order to eliminate the persisting cross interference of NO, the use of a reactive cover layer for enhancing the hydrocarbon selectivity of the sensor devices has also been tested. The earlier work [13] has been expanded to include the study of pulsed laser deposited (PLD) thin films.

Experimental

From the precursor materials $SrCO_3$, TiO_2, and Fe_2O_3, the *p*-type semiconductor $Sr(Ti_{0.8}Fe_{0.2})O_{3-\delta}$ (STF20) was prepared following the mixed oxide route. After calcination at 1200°C, the powders were ball-milled until yielding a particle size of 1.4 μm, as determined by laser diffraction on a Mastersizer 2000 (Malvern Instruments). Phase purity of the samples was assured by XRD measurements on a diffractometer (Philipps X'Pert-MPD-PW3040/00) with Cu–K-α radiation ($10° \le 2\Theta \le 90°$).

To prepare thick film samples on alumina substrates, a $SrAl_2O_4$ underlayer was screen-printed first as described in Ref. 14. This diffusion barrier prevents interactions of the STF20 film with the alumina substrate. Then, the STF20 film was deposited on top and sintered at 1100°C. The film thickness after sintering ranged from 15 to 25 μm.

For the pulsed laser deposition (PLD) of thin films, a pressed pellet was prepared from the same STF20 powders described above and densely sintered at 1520°C. This as-prepared target was used to deposit thin films on substrates of polycrystalline alumina equipped with IDC structures as described below. An excimer laser (KrF Lambda Physik, LPX305*i*) with wavelength λ = 248 nm, at a pulse frequency of 8 Hz, and energy of 600 mJ was used to deposit the films. The energy fluence at the target was estimated to be ~1.6 J/cm^2. Depositions were carried out under an oxygen atmosphere at a partial pressure of 13 Pa, with a heated substrate held isothermally at 700°C. After annealing at the same temperature for 30 min under an oxygen partial pressure of 53 kPa the films were cooled to room temperature at 10°C/min. From previous calibrations, thickness of the films was estimated to be 200 nm.

For measurements on sensor performance, the specimens were mounted in a custom built apparatus which permits loading of up to four sensors simultaneously. Heating to the desired operating temperature was achieved in a tube furnace. For sample gas delivery, different test gas species were added to a reference nitrogen flow containing 20 vol% of oxygen using mass flow controllers. The total gas flow was adjusted to 600 ml/min. In addition to the actual values of the mass flow controllers, the gas composition, and in particular the hydrocarbon content, was verified analytically by using a flame ionization detector (FID, Fisher Rosemount, NGA 2000). Prior to the measurement, samples were equilibrated for 20 min in nitrogen with 20% oxygen. Keeping this as a base gas, 500 ppm of the respective analyte gases, i.e. of propane, propene, a mixture of hydrocarbons (containing ethane, ethene, acetylene and propene in equal proportions), NO, and CO, were added. In the case of hydrogen, a concentration of 1000 ppm was used. During some measurements, oxygen sensor output response was also determined by reducing the oxygen content from 20 to 10%. The sensor response was studied at various temperatures ranging between 300 and 450°C. In all cases, the sensor response was measured as a conductometric change, with the dc resistance of the sensors being registered as a function of time using a Keithley 2700 digital multimeter.

Different metal electrodes and electrode configurations were also investigated. Figure 1 shows two types of electrode configurations predominantly used in measurements of STF20 thick film sensors with a set of four electrodes (Au or Pt) screen-printed beneath (Fig. 1a) and on top of the film (Fig. 1b).

The thin films display a significantly higher base resistance than the thick films as a result of the lower film thickness. Consequently, electrodes with an IDC structure were adopted to provide a parallel connection of multiple sensor units with a small electrode spacing, and thereby to decrease the overall resistance values. The alumina transducers for thin film depositions were either equipped with

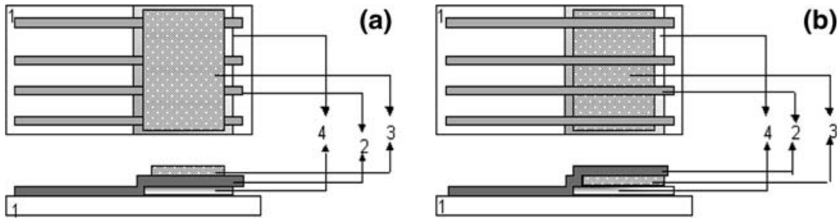

Fig. 1 Two-dimensional depictions of the electrode configurations used to test the STF20 thick films. (**a**) Bottom electrodes, (**b**) top electrodes. Numbers indicate: 1. Alumina substrate, 2. Pt- or Au-electrode, 3. STF20 thick film, and 4. $SrAl_2O_4$ buffer layer

screen-printed Pt-IDC structures (electrode spacing: 150 µm) or with photolithographic Au-IDC structures (electrode spacing: 12.4 µm).

In Table 1, an overview of the electrode configurations investigated for the thick/thin film combinations is shown.

In addition, the impact of a zeolite cover layer on top of the gas-sensitive STF film was investigated. The zeolite used was commercially available ZSM-5 powder (AlSi Penta, SN27), which has a doping of 1.62 wt% platinum according to the method described elsewhere [15]. Due to the used methods of ion-exchange, calcination and reduction, the cation ratio in the zeolite is known to be 85% Na^+ to 15% H^+. A paste of the zeolite powder has been deposited on top of screen-printed thick films, and on the surface of some selected thin films. After drying at 100°C and a sintering step at 450°C, a porous cover layer is obtained as presented in Fig. 2.

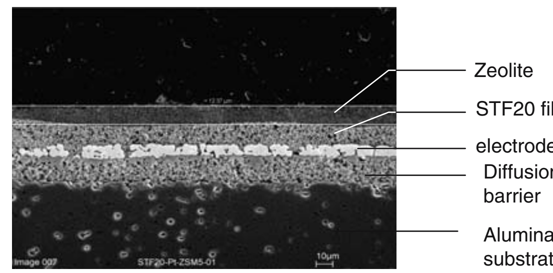

Fig. 2 SEM cross-section of an STF20 sensor with $SrAl_2O_4$ diffusion barrier and ZSM-5 cover layer

Results

In order to compare the hydrocarbon sensor performance, two parameters relating sensor output and the degree of cross interference are used in the following discussion. The sensor output response S, in this case represented by the relative change of the resistance [16], is calculated according to Eq. 1

$$S_{\text{test gas}} = \frac{R_{\text{test gas}} - R_0}{R_0} \tag{1}$$

with R_0: base resistance in dry air

$R_{\text{test gas}}$: resistance when exposed to the respective test gas

Table 1 Overview of the different electrode configurations

	Thick films		Thin films
Au	Screen-printed electrodes on top		Photolithographically structured IDC, beneath
Pt	Screen-printed electrodes	On top Beneath	Screen-printed IDC beneath

Sensor films: All prepared from STF20 on alumina substrates

For the evaluation of cross interference, the cross sensitivity factor *CSF* is introduced by Eq. 2. As the key component for comparison, the saturated hydrocarbon species propane (C_3H_8) has been selected for the thick films, whereas the unsaturated hydrocarbon species propene (C_3H_6) has been selected for the thin films.

$$\mathrm{CSF}_{\text{test gas}} = \frac{\Delta R_{500\text{ ppm test gas}}}{\Delta R_{500\text{ ppm key gas}}} = \frac{R_{500\text{ ppm test gas}} - R_0}{R_{500\text{ ppm key gas}} - R_0} \tag{2}$$

with $R_{500\text{ ppm test gas}}$: resistance when exposed to 500 ppm of the respective test gas

If $CSF > 1$, the sensor responds more to the test gas than to the key component propane, i.e., the cross sensitivity of the gas is high. Consequently, the lower the *CSF* value, the less prominent is the cross interference of the respective test gas.

STF20 thick films

Response of different electrode configurations

In Fig. 3, the resistance traces of a cross sensitivity measurement conducted at 400°C on thick film sensors with different electrode configurations are presented. The electrode configurations have shown profound impact on the sensor performance. Whereas the films equipped with platinum electrodes either underneath or on top of the sensitive film do not show a pronounced cross sensitivity towards CO or hydrogen, the resistance of the sensor with gold electrodes increases notably when exposed to these gases. Consequently, the use of gold electrodes is disadvantageous for the fabrication of selective hydrocarbon sensors based on STF compositions.

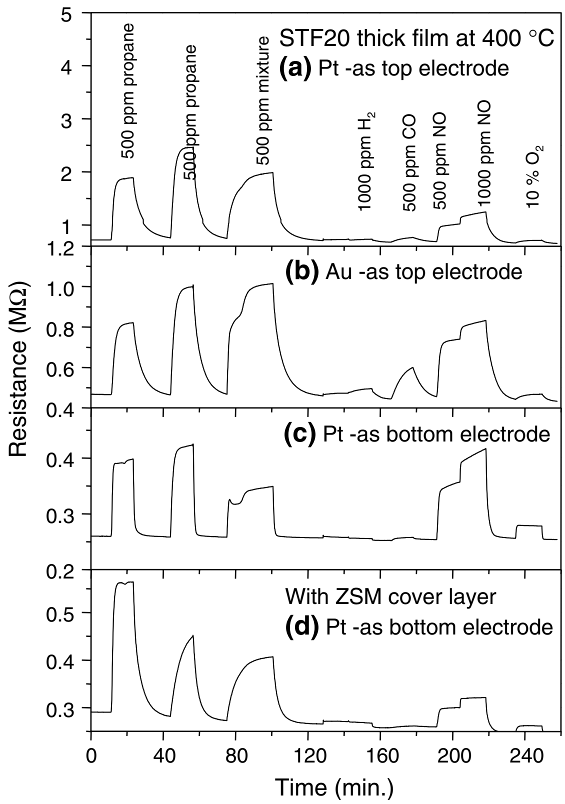

Fig. 3 STF20 thick film response to various gases under differing electrode configurations (**a–d**): response of the film with ZSM-5 as a cover layer with Pt-electrodes underneath the film. Operating temperature: 400°C, gas concentration as indicated, balance: dry air

In either case, NO was found to cause the most prominent cross interference. Table 2 compares the sensor output response *S* as defined by Eq. 1 as well as the *CSF* values for the different gases. The gas concentration was adjusted to 500 ppm for each gas.

First, only the uncovered sensor films are considered. According to the results represented in Fig. 3a–c and Table 2, hydrocarbon (HC) response was found to be the most pronounced with the Pt electrodes on top of the thick film. This configuration also presents a very low CSF_{NO} value, i.e., the lowest cross interference of NO. In either case, the plain sensor films show a somewhat higher response towards the unsaturated hydrocarbon species propene at 400°C. This observation corresponds to the findings reported in [13] for the STF40 composition, indicating that the members of the material family $SrTi_{1-x}Fe_xO_{3-\delta}$ behave similarly.

Application of a zeolite cover layer

Earlier results [13] were promising with regard to the use of a zeolite cover layer on top of the gas-sensitive STF film to promote selectivity.

Cross sensitivity measurements indicated an improved selectivity towards propane. Nevertheless, an increase in the sensor response time was observed because the zeolite cover acts as a barrier for the gas molecules penetrating through the zeolite film to the sensor underlayer.

According to an additional study that was conducted for identifying an optimum zeolite layer thickness [17], a 50 µm thick ZSM-5 film leads to optimum results with respect to response time and cross sensitivity. Although this thickness is not sufficient to eliminate the cross interference of NO completely, the latter is reduced without significantly delaying the sensor response time. In Fig. 2d and Table 2, the results for a conventional STF20 film (Pt electrodes underneath) covered with such a zeolite layer are shown. They indicate a pronounced selectivity of the device towards propane without deteriorating the response time towards this gas.

There is a significant advantage in combining the Pt electrode configuration on top of the sensor film with the 50 µm thick ZSM-5 cover layer. Figure 4 shows the resistance traces of two STF20 thick films equipped with Pt electrodes on top. In addition, one of the sensors has been modified with a zeolite coating as described above. The sensors were operated at 450°C and exposed to various saturated hydrocarbon species, ranging from methane (CH_4) to butane (C_4H_{10}). As unsaturated hydrocarbons, propene as well as the HC mixture described in the experimental section were used. For a better comparison of the different HC species, their concentration was adjusted so that the total number of carbon atoms $c_{TCA}= n\cdot c(C_nH_m)$remained the same. The gas composition was monitored with the FID. Cross interference of hydrogen, CO, and NO was tested as well.

As expected from former results, the zeolite efficiently reduces the NO cross interference without notably influencing the hydrogen or CO response. In addition, it enhances the sensor response towards all saturated hydrocarbons.

Table 2 Sensor output response S as defined by Eq. 1 and cross sensitivity factors CSF of thick films calculated from the results presented in Fig. 3 for different gases (concentration: 500 ppm)

	S/%			CSF values	
	Propane	Propene	NO	Propene	NO
Pt-top	164	244	42	1.5	0.26
Au-top	76	114	59	1.5	0.77
Pt-bottom	53	63	37	1.2	0.69
Pt-bottom with the zeolite cover	94	54	3	0.57	0.03

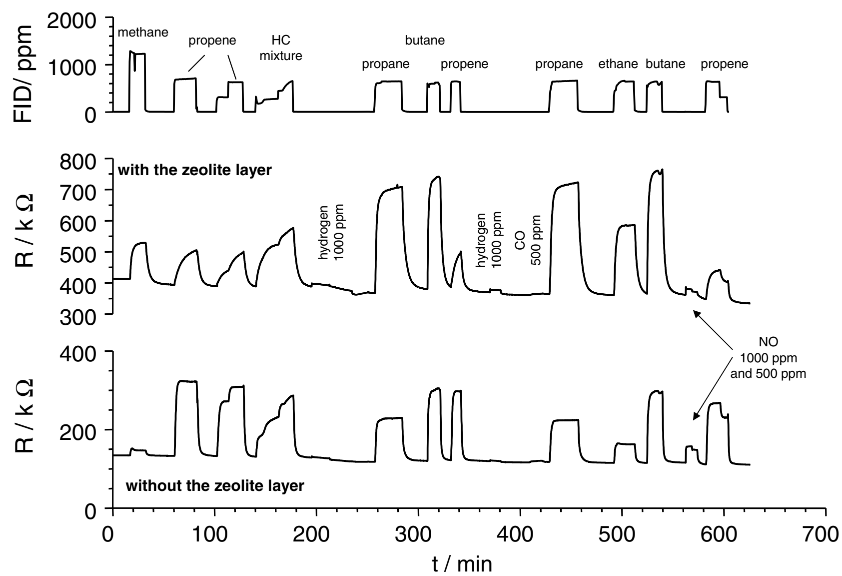

Fig. 4 Resistance traces of STF20 thick film sensors with and without the zeolite cover layer. Operating temperature: 450°C, gas concentration as indicated, balance: dry air. The result of the FID analysis of the sample holder exhaust is given for comparison

Noteworthy with the present STF20 thick film is that the sensor response is highest for butane (C_4H_{10}) and decreases subsequently with decreasing carbon chain length of the saturated hydrocarbons. At the same time, the sensor output response towards the unsaturated hydrocarbons decreases significantly compared to the uncovered thick film.

STF20 Thin Films

Sensor response with Pt and Au electrodes to saturated and unsaturated hydrocarbons

The morphology of the STF20 thin films grown by PLD onto the sensor substrates is significantly different to that of the thick films prepared by screen printing [13]. The thin films are relatively dense and low in porosity, with nano-meter grain sizes and low film thickness. Responses for STF20 thin films upon exposure to the different test gases were measured with Pt or Au-IDC electrodes underneath the films, and Fig. 5 shows this data for STF20 at 425°C for each electrode configuration. Overall, the base electrical resistance of STF20 films with photolithographically structured Au-electrodes decreases from the Pt-IDC type by about 2 orders of magnitude due to the smaller finger geometry and spacing. In Table 3, the corresponding *CSF*-values for the different cross interfering gases are represented.

With a Pt-IDC electrode, the sensor strongly responds to unsaturated hydrocarbons, whereas it shows only a small response towards 500 ppm propane ($CSF_{propane} << 1$). Similarly, it is relatively insensitive to 500 ppm NO or 1000 ppm H_2 but shows a higher response to the hydrocarbon mixture of ethane, ethene, acetylene and propene, and to some extent to 500 ppm CO ($CSF_{CO} = 0.25$). Sensors with Au-electrodes (Fig. 5b) as a comparison, show in

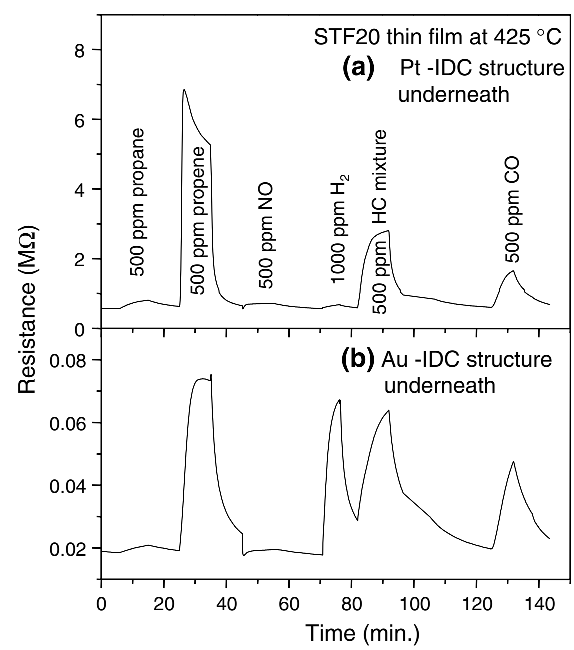

Fig. 5 Cross-sensitivity of STF20 thin film deposited using PLD at 425°C with two different types of metal electrodes underneath the film. (**a**) Pt-IDC, and (**b**) Au-IDC

addition a stronger response to 1000 ppm H_2, and also an enhanced response to the 500 ppm hydrocarbon mixture and 500 ppm CO, while the response to 500 ppm propane and NO is further diminished. This sensor configuration is less selective and presents a pronounced cross-sensitivity to CO in particular. It appears that the catalytic activity in Pt improves selectivity toward the more reactive species of unsaturated HCs. From this perspective, Pt-IDC electrode structures provide more selectivity for STF20 thin films than Au-electrodes, which is in accordance with the findings for thick film sensors. Due to this, subsequent

Table 3 Cross sensitivity factors *CSF* of thin films calculated from the resuilts presented in Figs. 5 and 6 for different gases (concentration 500 ppm)

	CSF values			
	Propane	NO	Hydrogen	CO
Pt-IDC, 425°C	0.07	0.04	0.04	0.24
Au-IDC, 425°C	0.05	0.02	0.88	0.53
Pt-IDC, 400°C	0.03	0.01	0.02	0.11
Pt-IDC, 400°C, with the zeolite cover	0.79	0.01	0.18	0.04

Propene has been chosen as the key gas

measurements on sensor responses were done with only Pt-IDC electrode structures.

STF20 thin films with Pt-IDC electrodes and Pt-ZSM-5 cover layer

Following a similar approach to that taken with the thick-films, the thin film STF20 sensors with Pt-IDC electrodes were also fabricated with a zeolite ZSM-5 layer deposited on top and measurements made to determine sensor response with the test gases.

Shown in Fig. 6 is a comparison of sensor response data for SFT20 thin films at 400°C with (Fig. 6a) and without (Fig. 6b) a zeolite cover layer on top of the films. The corresponding CSF-values are given in Table 3. As Fig. 6a

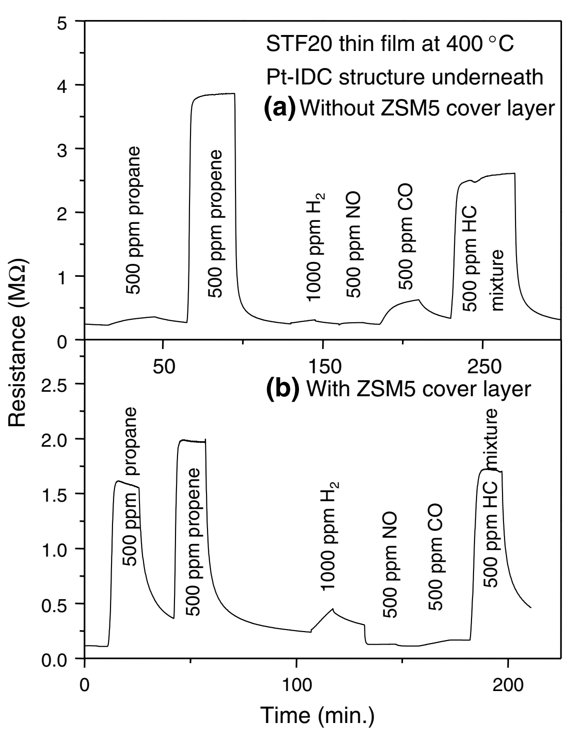

Fig. 6 Responses and cross-sensitivities of STF20 thin film having Pt-IDC structure underneath, (**a**) without and (**b**) with a cover layer of ZSM-5 on top of the film

reveals, STF20 thin films without the ZSM-5 layer show a reduced response towards 500 ppm CO and almost no response to 500 ppm propane, NO and 1000 ppm H_2. This data is similar, as expected, to that shown in Fig. 5a for a sensor in an equivalent configuration, but measured at 425°C.

With the ZSM-5 cover layer applied to the STF20 thin film, the cross-sensitivity to CO is almost completely eliminated (Fig. 6b, $CSF_{CO} << 1$). The response to 500 ppm saturated hydrocarbons, however, increases, and there is also an enhanced response to 1000 ppm H_2. It is likely that the Pt catalytic activity in ZSM-5 is different for saturated and unsaturated hydrocarbons species. This implies that a higher quantity of Pt doping in ZSM-5 or a larger overlayer thickness may improve selectivity to specific hydrocarbons given that a greater thickness of the ZSM-5 cover layer does increase selectivity in the case of STF thick films [17].

Discussion

The different behavior between Au and Pt electrodes that was observed for thick and thin film configurations can be readily explained by the higher catalytic activity of platinum. Very reactive reducing gases such as hydrogen or CO are almost entirely oxidized on the platinum electrodes and do not reach the sensor film. As a consequence, sensor films equipped with Pt electrodes do only exhibit a small response to these gases. In the case of Au electrodes, however, the concentration of H_2 and CO reaching the sensor film is not significantly affected, leading to a resistance change of the sensor film.

In order to explain the effect of the electrode position (i.e., on top or underneath the gas sensitive film) on the gas-sensing properties, one has to take into account the diffusion-reaction mechanism proposed previously [13].

In analogy to *n*-type metal oxide sensors, an oxygen adsorption layer is always present on the STF20 sensor surface surrounding the particles. When reducing agents, i.e. hydrocarbons C_nH_m, arrive on the catalytically active sensor surface, they react with the adsorbed oxygen or with labile oxygen in the bulk material. In this process, defect electrons (holes) are consumed, which leads to an increase in resistance. To cause a notable resistance change in thick films, the gas components need to penetrate deeply into the porous structure in order to react with the total film bulk. The complete process is thus described by the following differential equation:

$$\frac{\partial c}{\partial t} = D_{\text{eff}} \frac{\partial^2 c}{\partial z^2} - kc^{\gamma} \tag{3}$$

In Eq. 3, c denotes the concentration of the gas component, D_{eff} the effective diffusion coefficient, k the reaction constant, γ the reaction order, and z the penetration depth from the surface into the film.

Solving this equation yields a concentration profile $c(z)$, i.e., a dependency between the local gas concentration c and the penetration depth z. Whereas at the upper surface of the sensor ($z = 0$), the local concentration is identical to the concentration c_0 in the surrounding atmosphere, the concentration at the bottom of the sensor film (z = film thickness d) is lower given that the reducing gas is partly consumed on its way through the pores.

When measuring the film resistance by means of the top electrodes, mainly the parts of the film exposed to a local concentration close to c_0 contribute to the total resistance change. A resistance measurement conducted with bottom electrodes, however, mainly involves film areas exposed to a lower local concentration, thus yielding a less pronounced resistance change.

When comparing the sensor output response of STF20 thick films towards saturated hydrocarbons the sensor response was found to be highest for butane (C_4H_{10}) and to decrease subsequently with decreasing chain length of the saturated hydrocarbons although the total concentration of carbon atoms $c_{TCA} = n \cdot c(C_nH_m)$ was kept constant.

Assuming that the general redox-reaction between hydrocarbons C_nH_m and oxygen, which takes place at the sensor surface,

$$\begin{aligned}&(4n+m)\cdot h^+ + \left(2n+\frac{m}{2}\right)\cdot \mathrm{O}^{2-}_{\mathrm{ads}} + \mathrm{C}_n\mathrm{H}_m \rightarrow\\ &\quad n\ \mathrm{CO}_2 + \frac{m}{2}\mathrm{H}_2\mathrm{O}\end{aligned} \tag{4}$$

is complete, the total amount of consumed defect electrons h^+ can be determined by Eq. 5

$$\begin{aligned}\left[h^+_{\mathrm{consumed}}\right] &= (4n+m)\cdot c(\mathrm{C}_n\mathrm{H}_m)\\ &= (4n+m)\cdot\frac{c_{\mathrm{TCA}}}{n} = \left(4+\frac{m}{n}\right)\cdot c_{\mathrm{TCA}}\end{aligned} \tag{5}$$

In the case of saturated hydrocarbons, where $m = 2n + 2$, Eq. 5 yields

$$\left[h^+_{\mathrm{consumed}}\right] = \left(6+\frac{2}{n}\right)\cdot c_{\mathrm{TCA}} \tag{6}$$

According to this formula, the theoretical resistance increase should be the more prominent the smaller the HC chain length, i.e., the smaller n. This contradiction indicates that the reaction kinetics are different for the various hydrocarbons. To more fully understand this process, additional catalytic studies on the material STF are therefore needed. In particular, the possible effects of this surface redox reaction on parallel reactions (e.g. the incorporation of chemisorbed oxygen into oxygen vacancies, which according to [18] is the rate determining step for oxygen stoichiometry changes of $SrTi_{1-x}Fe_xO_{3-\delta}$) need to be investigated in detail.

In order to explain the reduction of the NO cross interference by the use of a zeolite cover, an initial catalytic study was conducted on the zeolite material. It was found that due to its high Pt content, the zeolite oxidizes NO to NO_2 and CO to CO_2. While passing through the porous zeolite cover, most of the NO or CO present in the gas phase is converted and does not reach the sensor surface.

Noteworthy with the present zeolite covered films is the contrary behavior observed for saturated HC (increased sensor output response) and unsaturated HC (decreased sensor output response). The reason for this opposition leading to a selective device for detecting saturated hydrocarbons is not yet clear. However, a catalytic conversion of the HC passing the zeolite layer is expected to take place in analogy to the NO or CO conversion. Ongoing studies are therefore aiming at investigating the catalytic properties of the zeolite towards saturated and unsaturated HC in more detail with respect to reaction products and kinetics.

Conclusions

STF20 thick films prepared using screen printing with Pt-IDC electrodes underneath the film and with the 50 μm ZSM-5 cover layer at 400°C act as better sensors to detect saturated hydrocarbons (e.g. propane or butane) than films with other electrode configurations and without the ZSM-5 layer. Sensor thin films of STF20 made using the PLD technique, possess high density. With Pt-IDC electrode structures underneath the thin film and without ZSM-5 overlayers, they are more strongly selective to unsaturated hydrocarbons (propene). With ZSM-5 as a cover layer, the thin films become insensitive to CO, but display increased cross-sensitivity effects from saturated hydrocarbons (e.g. propane). The role of the highly catalytically active Pt, either as a component of the electrodes or in the Pt doped zeolite cover layer, is key to imparting sensor functionality and to modify or enhance selectivity of the gas sensitive film. The competitive catalytic reaction versus diffusional properties of the analyte gas species with the different layers in the sensor configuration are important factors to be considered in sensor design.

Acknowledgements The authors thank Hans-Jürgen Deerberg for SEM pictures, Monika Wickles for the help in sample preparation, Andreas Dubbe and Gunter Hagen for zeolite preparation, and Petra Kuchinke (Univ. of Bayreuth) for catalytic studies. Thanks are due to Xiaomei Du of ICPET-NRC for the help in thin film deposition using PLD. This project was supported by the joint international program, National Research Council of Canada and the Helmholtz Gemeinshaft (project NRCC-21-CRP-02 and 01SF02001 9.2). Financial support of German Federal Ministry of Education and Research (BMBF) is also gratefully acknowledged.

References

1. Moseley PT, Williams DE (1989) Polyhedron 8:1615
2. Barsan N, Schweizer-Berberich M, Gopel W (1999) Fresenius' J Anal Chem 365:287
3. Goepel W, Schierbaum KD (1995) Sens Actuators B 26:1
4. Traversa E, Bearzotti A, Miyayama M, Yanagida H (1998) J Eur Ceram Soc 18:621
5. Lin F, Takao Y, Shimizu Y, Egashira M (1995) Sens Actuators B: Chem B25:843
6. Meixner H, Lampe U (1996) Sens Actuators B: Chem 33:198
7. Williams DE (1999) Sens Actuators B: Chem 57:1
8. Yannopoulos LN (1987) Sens Actuators 12:263
9. Niemeyer D, Williams DE, Smith P, Pratt KF, Slater B, Catlow CRA, Stoneham AM (2002) J Mater Chem 12:666
10. Li Y, Wlodarski W, Galatsis K, Moslih SH, Cole J, Russo S, Rockelmann N (2002) Sens Actuators B: Chem 83:160
11. Martinelli G, Carotta MC, Ferroni M, Sadaoka Y, Traversa E (1999) Actuators B: Chem 55:99
12. Sahner K, Moos R, Matam M, Post M (2003) In: Proceedings of IEEE sensors 2003. Toronto, Canada, pp 926–931
13. Sahner K, Moos R, Matam M, Tunney J, Post M (2005) Sens Actuators B: Chem 108:102
14. Moos R, Rettig F, Hürland A, Plog C (2003) Sens Actuators B: Chem 93:42
15. Canizares P, De Lucas A, Valverde JL, Dorado F (1997) Ind Eng Chem Res 36:4797
16. D'Amico A, Di Natale C (2001) IEEE Sens J 1
17. Sahner K, Moos R, Matam M, Post M (2005) In: Sensor 2005, proceedings vol I, May 2005. Nuernberg, Germany, pp 201–206
18. Merkle R, Maier J (2005) In: International conference on solid state ionics, SSI-15, book of abstracts, July 2005. Baden-Baden, Germany, p 63